Solar-Terrestrial Physics. 2025, vol. 11, iss. 4, pp. 29–38. DOI: 10.12737/stp-114202502. © 2025 R.V. Vasiliev, I.K. Edemskiy, A.D. Shelkov, M.F. Artamonov, S.S. Alsatkin, U.N. Evseev, V.P. Lebedev, V.P. Tashlykov, A.V. Tashchilin, A.V. Timchenko. Published by INFRA-M Academic Publishing House

DOI: 10.12737/stp-114202502

Received March 27, 2025
Accepted July 14, 2025

ANALYZING THE BEHAVIOR OF MID-LATITUDE UPPER ATMOSPHERE IONOSPHERIC PLASMA AND AIRGLOW I_{630} FROM IS RADAR AND FABRY—PEROT INTERFEROMETER DATA

R.V. Vasiliev
Institute of Solar-Terrestrial Physics SB RAS, Irkutsk, Russia, roman_vasilyev@iszf.irk.ru

I.K. Edemskiy
Institute of Solar-Terrestrial Physics SB RAS, Irkutsk, Russia, ilya@iszf.irk.ru

A.D. Shelkov
Institute of Solar-Terrestrial Physics SB RAS, Irkutsk, Russia, alshel@iszf.irk.ru

M.F. Artamonov
Institute of Solar-Terrestrial Physics SB RAS, Irkutsk, Russia, artamonov.maksim@mail.iszf.irk.ru

S.S. Alsatkin
Institute of Solar-Terrestrial Physics SB RAS, Irkutsk, Russia, alss@iszf.irk.ru

U.N. Evseev
Yu.G. Shafer Institute of Cosmophysical Research and Aeronomy SB RAS, Yakutsk, Russia, Evseev@ikfia.ysn.ru

V.P. Lebedev
Institute of Solar-Terrestrial Physics SB RAS, Irkutsk, Russia, lebedev@iszf.irk.ru

V.P. Tashlykov
Institute of Solar-Terrestrial Physics SB RAS, Irkutsk, Russia, vtashlykov@iszf.irk.ru

A.V. Tashchilin
Institute of Solar-Terrestrial Physics SB RAS, Irkutsk, Russia, avt@iszf.irk.ru

A.V. Timchenko
West Department of Pushkov Institute of Terrestrial Magnetism, Ionosphere and Radio Wave Propagation RAS, Kaliningrad, Russia, aleksandr.timchenko77@gmail.com

Abstract. The dynamics of the parameters of ionized and neutral components of Earth's upper atmosphere at midlatitudes near the equinox was studied for several days under quiet geomagnetic conditions. The ionospheric parameters were obtained by an incoherent scatter radar; the parameters of the neutral atmosphere at ionospheric altitudes, from characteristics of the atomic oxygen glow at a wavelength of 630 nm with a Fabry—Perot interferometer. Synchronous variations similar in relative amplitudes were detected in the glow intensity and plasma concentration, the nature of which was explained using numerical modeling, as well as a combination of model and empirical data. It is shown that the vertical wind effect is of decisive importance for the vertical transport of plasma and the enhancement of the atomic oxygen glow in the period of time considered. The phenomenon under study was associated with the midnight temperature maximum, which was first observed at 52° N. A method for calibrating optical measurements using radiophysical data is presented in the approximation of the dominant role of plasma parameter variations over neutral atmosphere parameter variations.

Keywords: ionosphere, thermosphere, airglow, electron density, Fabry—Perot interferometer, incoherent scatter radar, numerical modeling, neutral wind, midnight temperature maximum.

INTRODUCTION

To date, Eastern Siberia has a well-developed instrumental radiophysical infrastructure for studying the ionized component of the upper atmosphere—ionosphere and its variations under the influence of the Sun and Earth's atmosphere. Networks of ionosondes [Cedric et al., 2022], GNSS receivers [Afraimovich et al., 2012], and the incoherent scatter radar [Zherebtsov et al., 2002] successfully function. The neutral component of the upper atmosphere, its composition, temperature, and dynamics play an important role in the processes controlling ionospheric plasma conditions [Van Zandt, 1967; Rishbeth, 1988]. Therefore, to gain a deeper understanding of ionospheric dynamics, it seems advisable to develop, simultaneously with radiophysical instruments, observations of the upper atmosphere chemiluminescence which provide information on physicochemical parameters of the neutral component [Weinstock, 1975; Shepherd et al., 1997; Garcia et al., 2000; Vasilyev et al., 2020].

Study of processes in the ionosphere and simultaneous analysis of radiophysical and optical manifestations can be carried out using numerical simulation methods [Namgaladze et al., 1981; Watanabe et al., 1986; Bryunelli, Namgaladze, 1988; Grigoryev, Latyshev, 1989; Korenkov et al., 1996]. The plasmasphere-ionosphere model developed at ISTP SB RAS (PIM ISTP) [Krinberg, Tashchilin, 1984] can calculate not only the con-

centrations of electrons N_e and basic ionospheric ions along a given geomagnetic field line under specified geomagnetic conditions, but also vertical profiles of volume airglow. Comparing variations in vertical profiles of N_e and volume airglow under the influence of variations in the input control parameters of the model makes it possible to evaluate their physicochemical relationships. The feedback, which can be used to set variations in the input parameters, can be a comparison of model characteristics with field data.

Synthesis of information on the dynamics of the mid-latitude upper atmosphere atomic oxygen glow intensity at a wavelength of 630 nm, recorded by an optical spectrometer [Mikhalev, 2018], and the N_e profile, obtained by an ionosonde [Ratovsky, Oinats, 2011], allowed the development of a photochemical model for reconstructing the atomic oxygen ion profile, which can explore new aspects of ionospheric dynamics [Duann et al., 2024]. At the moment, these models do not contain parameterizations related to the upper atmosphere dynamics, tidal and wave phenomena, as well as to geomagnetic events, so it makes sense to continue research (to further develop them, using a wider range of instruments) into the joint dynamics of the ionized and neutral components of the upper atmosphere.

In addition to the ionosonde and spectrometer, incoherent scatter radars can be employed to find the vertical profile of plasma concentration both below and above its maximum, as well as full-sky cameras and Fabry—Perot interferometers (FPI) can be used to identify spatial variations in airglow, temperature, and horizontal wind velocity of the neutral component. The results of observation of the dynamics of spatial variations in the 630 nm airglow and the horizontal wind in this airglow layer together with the results of observation of the dynamics of spatial variations in the N_e profile were analyzed in [Otsuka et al., 2003]. The large-scale wave of airglow brightness observed at near-equatorial latitudes was associated with ionospheric plasma descending under the influence of the poleward meridional wind. The authors suggested that this phenomenon is linked to the midnight temperature maximum (MTM) in the equatorial thermosphere.

MTM is usually observed in the equatorial upper atmosphere [Colerico, Mendillo, 2002]. It is accompanied by an increase in pressure, is defined by a weakening or change of the direction of the meridional wind to the pole, spreads poleward, and has two secondary maxima near a latitude ±15°. As MTM propagates, it reaches mid-latitudes. For example, Colerico and Mendillo [2002] report that its passage was observed by all-sky cameras at the El Leoncito Observatory (31.8° S, 69.0° W), noting that this latitude should not be considered the MTM propagation limit. The authors also point out that the efficiency of the meridional wind in vertical transport of plasma decreases with increasing latitude, and their observations at Millstone Hill demonstrate a much less pronounced manifestation of MTM in optical observations.

In a more recent paper [Mesquita et al., 2018], the authors analyze data from the FPI network located in the United States in the latitude range 35–45° N. By approximating background temperature values with a combination of 24, 12, and 8 hr harmonics and applying a 2D-inversion algorithm, they obtain 2D maps of temperature variations in 30-min increments, which give insight into the spatial and temporal structure of MTM. Thus, it is reported that the main MTM peak is often preceded by an additional evening peak 4.5 hrs in advance, although features of this two-peak structure vary from night to night. Presenting seasonal observation statistics, the authors, without estimating the latitude limit, conclude that MTM can be observed up to at least 44.4° N.

This paper describes the results of optical and radiophysical observations of changes in the altitude structure of characteristics of the upper atmosphere and ionosphere. The observations were carried out as part of the scientific and educational intensive of the Baikal Young Scientists' International School on Fundamental Physics (BSFP) "Physical Processes in Outer and Near-Earth Space" and the XVII Young Scientists' Conference "Interaction of Fields and Radiation with Matter" (Irkutsk, September 5–10, 2022). Participants of the intensive worked at ISTP SB RAS unique research facilities such as the Irkutsk Incoherent Scatter Radar (IISR) [Zherebtsov et al., 2002] and Optical instruments of the National Heliogeophysical Complex of the Russian Academy of Sciences (NHC RAS) [Zherebtsov, 2020].

INSTRUMENTS AND DATA

Irkutsk Incoherent Scatter Radar

Ionizing radiation from the Sun produces charged particles in the neutral atmosphere: ions and electrons. Their largest number is recorded at altitudes 50–1000 km in the layer called the ionosphere. Identification of height and time variations of charged particle concentrations and temperatures allows us to examine the dynamics of the ionosphere and is made by various (mainly radiophysical) instruments around the globe. Maximum N_e is observed at altitudes 200–400 km (F2 layer), where the main ionizable component is atomic oxygen [Hargreaves, 1982].

The Irkutsk Incoherent Scatter Radar (IISR) of the ISTP SB RAS Observatory of Radiophysical Diagnostics of the Atmosphere (52.9° N, 103.3° E) is the only radiophysical complex in Russia that can determine parameters of the entire thickness of the ionosphere with the IS method [Zherebtsov et al., 2002]. The method is based on the analysis of effects of high-frequency electromagnetic wave scattering (frequency is higher than the plasma one) by weak plasma permittivity fluctuations at ionospheric heights and allows us to reconstruct its parameters such as electron and ion concentrations and temperatures T_e, T_i [Alsatkin et al., 2015]. Rotation of the IISR plane-polarized electromagnetic sounding wave in ionospheric plasma (Faraday effect) leads to fading of the received radar signal, which yields absolute N_e. For this purpose, the least squares method is exploited to select parameters of the function describing the vertical power profile of the received radar signal. The parameters of the function are the vertical N_e profile, the zenith angle, the altitude variation of the Faraday rotation phase, the electron gyrofrequency, the radar

operating frequency, and the angle between radar beam and geomagnetic field vector.

NHC RAS Fabry — Perot interferometers

The atomic oxygen glow in the 630 nm red line is formed at altitudes ~200–400 km due to the transition of atoms from the excited state O(1D) to the ground state O(3P) [Shefov et al., 2006]. Excited atoms are generated mainly as a result of dissociative recombination reaction and collisions of oxygen atoms with thermal and superthermal electrons [Tashchilin, Leonovich, 2016]. Thus, the 630 nm airglow intensity I_{630} contains information on the number of excited oxygen atoms that depends on N_e at the airglow height.

On the territory of the ISTP SB RAS Geophysical Observatory (GPhO ISTP) in the Tory village (51°48′ N, 103°04′ E), NHC RAS aeronomic FPIs are used to observe different characteristics of the natural night airglow [Vasilyev et al., 2020]. Observations of the 630 nm red line glow provide data on variations in atmospheric temperature and wind speed at an altitude ~250 km. The key feature of FPI is the application of the multipath interference principle that makes it possible to determine the Doppler shift and broadening of the observed line, which are utilized to find the temperature (up to 5–15 K) and velocity (up to 2–4 m/s) of the luminous neutral component of the upper atmosphere. Adopting the method [Harding et al., 2014] to primary data from interferometers [Vasilyev et al., 2017] allowed us to identify, along with the horizontal wind velocity and temperature, the integral (over height) airglow intensity in the observed line and the variation in the vertical velocity of the luminous neutral component. However, the proposed new method of analyzing observational data does not permit us to directly obtain the absolute intensity as a volume emission rate or nonsystemic (rayleigh, R) airglow characteristic. Moreover, the vertical velocity variation is not absolute either. Therefore, comprehensive studies of the upper atmosphere with such characteristics require photometric calibration of these instruments and additional information on the vertical transport of upper atmosphere air.

Interval and conditions of observations

The scientific and educational intensive was held immediately before the main BSFP events on August 29 – September 1, 2022. It was during this period that radiophysical and optical instruments made simultaneous observations. Geomagnetic conditions in this period were quiet (K_p~2, Dst~±15), a weak storm (Dst~–70) began only on September 3. For optical observations, the conditions were determined by the number of stars in the field of view of a surveillance camera [Podlesny et al., 2022]. According to this criterion, observations during the nights on August 29–30 and 30–31 were performed under variable cloudiness conditions.

The interferometer takes measurements at the zenith and in the directions of the cardinal points at an angle of 45° above the horizon. IISR carries out observations with a deviation from the vertical of 16° to the west and ~25° to the south, southwest. The observatories with the radar and the interferometer are spaced along the meridian by ~130 km, with IISR located to the north, northeast of FPI. Thus, the vertical direction of FPI observations and the inclined southerly direction of IISR observations can be roughly considered as observations of the same region of the atmosphere. In addition, with some assumptions (~100 km), the quasi-vertical direction (16°) of IISR observations and the northerly direction of FPI observations may be thought to provide the same observation conditions.

Figure 1 illustrates variations in N_e (blue curve) at an altitude of 265 km (according to IISR data, in quasi-vertical direction, 16°) and in the integral airglow intensity (red curve) in the I_{630} line (according to FPI data, northerly direction) for the period under study. The gray area is the range of changes in N_e at altitudes 250–280 km. The choice of the altitudes is due to the fact that the atomic oxygen glow for the season and geomagnetic activity level of interest, according to the ISTP plasmasphere-ionosphere model (PIM ISTP) data, occurs in a layer located in this range, which generally corresponds to the characteristics of the airglow layer [Shefov et al., 2006]. During the simultaneous observations (local night), the N_e and I_{630} curves show similar variations, which may indicate the presence of a connection between them.

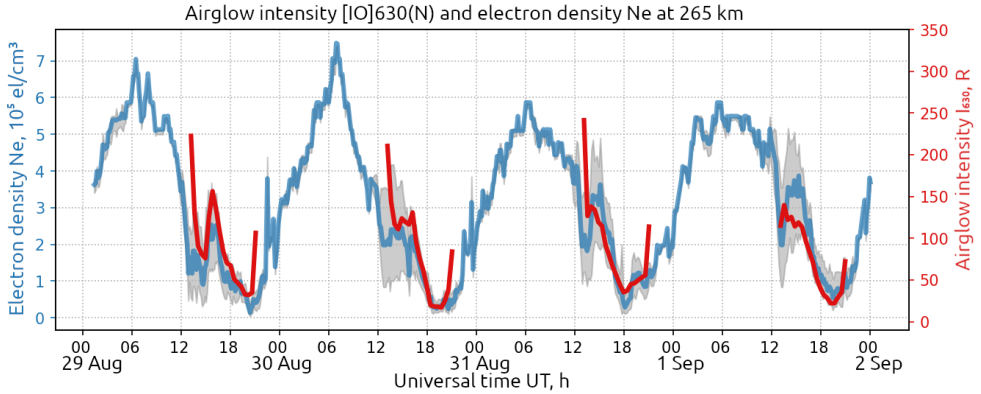

Figure 1. Variations in the electron density N_e according to IISR data at an altitude of 265 km (blue curve) and in the red line airglow intensity I_{630} (red curve) according to FPI data for the period August 29 – September 1, 2022. The range of N_e variations at altitudes 250–280 km is highlighted in gray

The purpose of this work is to determine the cause of the observed synchronous variations, the causes of the synchronous dynamics of N_e and I_{630}, and to assess the possibility of photometric calibration of FPI, using information from radiophysical instruments.

DATA ANALYSIS

Numerical model PIM ISTP can identify vertical profiles of concentration and temperature of the main ionospheric charged components along the dipole geomagnetic field line above 100 km [Krinberg, Tashchilin, 1984]. The simulation results allow us to estimate the concentration of excited oxygen atoms and hence volume and integral airglow intensities. Such calculations were performed for August 29 – September 1, 2022. Figure 2 shows vertical profiles of N_e in the altitude range 150–600 km, calculated by PIM ISTP (*a*) and measured by the IS radar (*b*), as well as the dynamics of the neutral wind components (*c*) according to the HWM07 model (dashed lines) and FPI data (nodal lines): zonal component (blue curves), meridional component (orange curves), and vertical component (green curves). Gray rectangles are time intervals with cloudiness over ISTP SB RAS GPhO. Due to scattering of radiation from the lower thermosphere with a wavelength of 630 nm by tropospheric clouds, observations of this scattered light in a particular direction will reflect the integrated (uneven cloud density) characteristics of thermospheric radiation above the clouds in a complicated way. Thus, the Doppler shifts of the center line contained in the data will have quasi-random components of different signs. Under such conditions, the horizontal wind speed will be determined incorrectly by the method of subtracting the Doppler shifts in clear sky radiation from opposite directions [Vasilyev et al., 2017]. Note that the calculated wind speeds (see Figure 2) are highly likely to be incorrect during periods marked with gray rectangles.

Differences in the diurnal dynamics of the vertical N_e profiles according to IISR and model data may be related, first of all, to the use of MSIS00 [Picone et al., 2002] and HWM07 [Alken et al., 2008] as models of neutral atmosphere parameters embedded in PIM ISTP. The quality of prediction of climatological parameters by HWM and MSIS has well-known problems for the region of interest [Shcherbakov et al., 2015].

The nature of the observed N_e profiles makes it possible to assume that the nocturnal features of their dynamics depend on the meridional wind and the vertical transport of the neutral component. The vertical plasma drift caused by the wind in the upper atmosphere can be estimated from the plasma equilibrium condition under the action of the Lorentz force, collisions of ionized particles with neutral particles, and the electric field E:

$$\begin{aligned} &e\vec{V}_i \times \vec{B} - m_i \nu \left(\vec{V}_i - \vec{U}_n\right) + e\vec{E} = 0, \\ &\vec{B} = \left(0,\, B_0 \cos I,\, B_0 \sin I\right). \end{aligned} \tag{1}$$

Here e is the electron charge; m_i is the mass of type i ion; V_i is the plasma drift velocity (type i ions); U_n is the

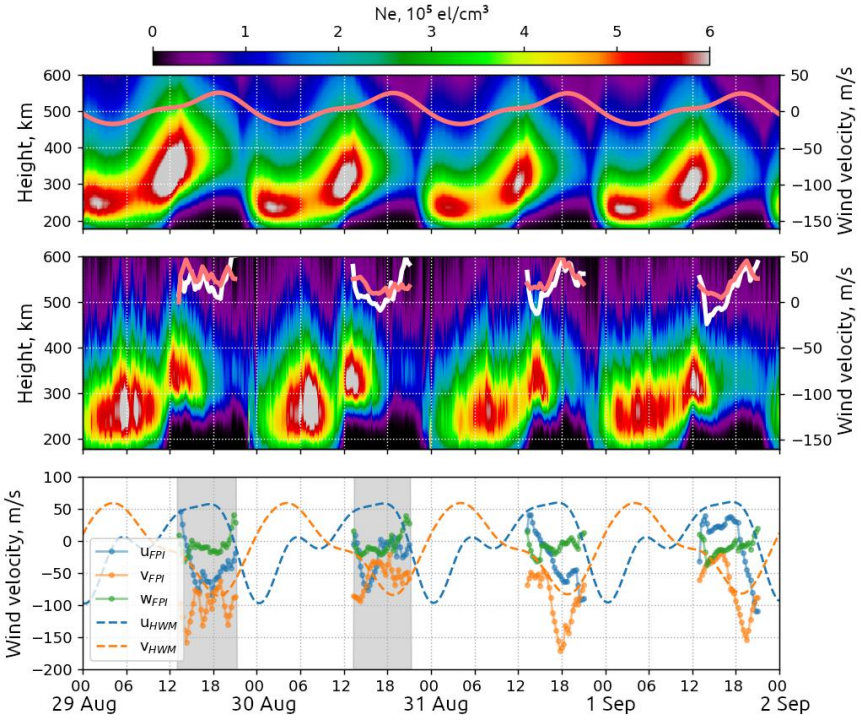

Figure 2. Electron density variations according to the ISTP SB RAS model (*a*) and IISR data (*b*). The pink line is the vertical drift velocity according to HWM (*a*) and FPI data (*b*). The white line is the vertical drift in terms of vertical transport of matter (W_{FPI}). Panel *b* illustrates variations of the zonal (U_{FPI}), meridional (V_{FPI}), and vertical (W_{FPI}) neutral wind components according to FPI data (lines with nodes), as well as in the zonal (U_{HWM}) and meridional (V_{HWM}) components as obtained by HWM (dashed lines). Gray rectangles are cloudy periods (large error in determining the wind) over ISTP SB RAS GPhO (Tory)

neutral wind speed; ν is the frequency of ion-neutral collisions. In this case, only the meridional $B_0\cos I$ and vertical $B_0\sin I$ components of the magnetic field B are considered significant, which allows us to uniquely determine them through magnetic induction B_0 and inclination I. Neglecting the electric field effect (E=0), we can simplify (1) to a system of equations and express the vertical component of electron drift velocity as

$$V_z = \frac{1}{1+r^2}\times$$
$$\times\left(r\cos I\cdot U + \sin I\cos I\cdot V + \left(r^2+\sin^2 I\right)W\right), \quad (2)$$
$$r = \frac{\nu}{\omega} = \nu\frac{m_i}{eB_0}.$$

Here U, V, and W are the zonal, meridional, and vertical neutral wind components. The parameter r is defined by the ratio of the cross-section of interaction between charged and neutral particles to their drift velocity under the influence of a magnetic field.

Using (2), we can estimate the ionospheric plasma drift velocity, using model and empirical data on the neutral component dynamics. The pink line (see Figure 2) indicates the change of the vertical drift velocity obtained from HWM07 horizontal wind data with zero vertical displacement (*a*) and from FPI measurements (*b*). The white line is the behavior of plasma drift according to (2) under the action of two horizontal wind components and the vertical motion variation as the vertical wind velocity W, which were obtained by the interferometer. Preliminarily, we can say that the vertical plasma drift obtained from interferometer data during the nights on August 31 and September 2 correlates fairly well with the vertical dynamics of ionospheric plasma from IISR. The minimum drift variation at ~15 UT coincides with the minimum height of the layer; and the maximum drift variation at ~18–19 UT, with the maximum height of the layer during these nights. Note that the airglow intensity increases simultaneously with an increase in N_e at ~15 UT at a minimum vertical drift velocity. It seems to be the downward motion of the neutral component that causes the ionospheric plasma to move and the number of excited oxygen atoms to grow (see Figure 1), thereby leading to an increase in the airglow intensity.

The electron density acts as a control parameter in all excited oxygen atom generation reactions, which emit the 630 nm airglow during transition to the ground state [Doering, 1992; Mantas, 1994; Tashchilin, Leonovich, 2016]:

- collisions with thermal electrons:

$$\left[\mathrm{O}(1\mathrm{D})\right] = 0.596\frac{9329+T_e}{\left(51813+T_e\right)^3}\times$$
$$\times\sqrt{T_e}\exp\left(-\frac{22576}{T_e}\right)\frac{[\mathrm{O}]N_e}{L_{630}}; \quad (3)$$

- dissociative recombination of molecular ions O_2^+:

$$\left[\mathrm{O}(1\mathrm{D})\right] = f(1\mathrm{D})1.95\cdot10^{-7}\left(\frac{300}{T_e}\right)^{0.7}\frac{\left[O_2^+\right]N_e}{L_{630}}; \quad (4)$$

- collisions of O atoms with superthermal electrons

$$\left[\mathrm{O}(1\mathrm{D})\right] = 4\pi\frac{[\mathrm{O}]}{L_{630}}\int_{E_{1D}}^{\infty} I_O^{(1D)}(E)\Phi_0(E)dE. \quad (5)$$

Here, the concentrations of electrons N_e, ions of [O] atoms, and oxygen molecules $\left[O_2^+\right]$ are given in cm^{-3}; the temperatures of electrons T_e and neutral particles T_n, in K; $I_O^{(1D)}$ is the differential cross-section for excitation of the 1D level by electron impact (cm^2); $F_0(E)$ is the isotropic part of the superthermal electron flux with energies from E to $E+dE$. The coefficient f(1D)=1.2 determines the efficiency of the formation of excited O(1D) atoms in the dissociative recombination reaction [Link, Cogger, 1988; Tashchilin, Leonovich, 2016].

The value L_{630} included in the denominator describes the nonradiative quenching of the O(1D) level in collisions with neutral particles O, O_2, N_2 (A_{1D}=0.00745 s^{-1}) [Kernahan, Pang, 1975; Berrington, Burke, 1981]:

$$L_{630} = A_{1D} + 10^{-11}\times$$
$$\times\left(0.16\,T_e^{0.91}n_e + 0.8[\mathrm{O}] + 2.9e^{\frac{68}{T_e}}[\mathrm{O}_2] + 2e^{\frac{108}{T_n}}[\mathrm{N}_2]\right). \quad (6)$$

The 630 nm airglow intensity (R) is defined as the integral of the total concentration of excited atoms contained in a given layer of heights h_1–h_2:

$$I_{630} = 10^{-6}A_{630}\int_{h_1}^{h_2}\left[\mathrm{O}(1\mathrm{D})\right]dh,$$
$$A_{630} = 0.00563\ c^{-1}. \quad (7)$$

The share of each process in the total integral value varies during the day. Numerical calculation of the concentration of charged and neutral components of the ionosphere together with Equations (3)–(7) allows us to observe this diurnal dynamics. Figure 3 illustrates 630 nm integral glow variations derived from (3)–(7) using the PIM ISTP results for the observation period of interest. Filled blocks mark the night time for ISTP SB RAS GPhO on the Earth surface (light blue) and 100 km above it (dark blue). As night falls, the contribution of the airglow from dissociative recombination (yellow dotted line) completely determines the integral intensity (bold red curve) and correlates with N_e at an altitude of 250 km (blue curve).

If we compare the night 630 nm line intensity variation measured by FPI (see Figure 1) and modeled by PIM ISTP (see Figure 3), we can see that there is no local intensity maximum around midnight (~16 UT). This discrepancy probably results from the above discrepancy between the parameters of observed and modeled ionospheric plasma, caused by the use of HWM07 in PIM ISTP to obtain vertical N_e profiles. Analysis of Figure 2 suggests that the lack of consideration of vertical air motion in the model leads to the absence of maximum N_e near local midnight on the dates under study.

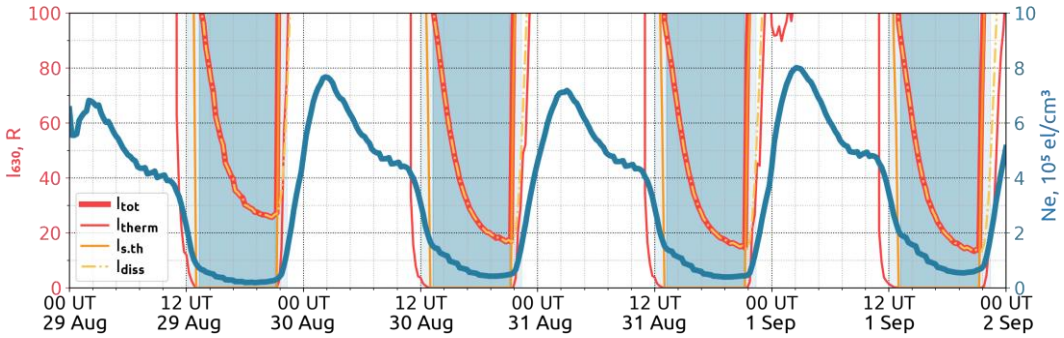

Figure 3. 630 nm atomic oxygen glow intensity (bold red curve) and N_e at an altitude of 250 km (blue curve) according to PIM ISTP. Thin lines indicate contributions of [O] reactions with thermal (thin red) and superthermal (thin yellow) electrons and dissociative recombination reactions (yellow dotted line). The beginning of night (the solar terminator at an altitude of 100 km) is marked with blue rectangles

We can therefore propose to employ empirical data on the parameters of the upper atmosphere to simulate airglow and then compare it with the results of optical observations.

Figure 3 shows that thermal and superthermal electrons make almost no contribution to the 630 nm night airglow during the observations analyzed in this paper. Hence, in modeling it is sufficient to take into account only the contribution of dissociative recombination of molecular oxygen ions. Among the parameters necessary for modeling (Equations (4), (6)), N_e has the largest amplitude of variations, which means that it should be considered as the main driver of airglow variability. Its diurnal relative variation is 50–60 %, whereas the remaining molecular oxygen components (N_n, N_i, T_n, T_i) vary by 10–25 %. Thus, to calculate the 630 nm atomic oxygen glow intensity, it is worthwhile using N_e observed by radiophysical methods.

The vertical N_e and T_e profiles can be obtained from IISR data; and the altitude distributions of other necessary parameters, from the models. The vertical profiles of molecular oxygen N_i is provided by IRI-2020 [Bilitza et al., 2022], of oxygen N_n, as well as its molecules and nitrogen molecules are available from the MSIS 2.1 model [Emmert et al., 2022]. The T_n profile can also be calculated in the MSIS model; however, FPI can determine the average temperature of the radiating layer. Since the intensity integral over height will eventually be used to compare model and empirical data, the temperature data obtained by the interferometer can be employed. Comparison of the contribution of the temperature profile and its value at the height of maximum of the radiating layer (280 km) from the MSIS 2.1 model to the integral intensity has revealed no significant difference. This suggests that the T_n dependence on height is not critical for calculating the integral 630 nm line emission intensity, which makes it possible to apply the FPI data on T_n to airglow modeling.

The modeling was performed for the northerly and zenith directions. Figure 4 shows that the model (blue curves) and empirical (red curves) night intensity variations correlate fairly well (Table).

The differences in the time variation mainly consist in the time shift in the local maxima of the obtained characteristics from ten minutes to several hours. The night sky on August 29 and 30 was covered with clouds, which does not allow us to use the results of FPI observations to obtain the horizontal wind, yet the cloud cover has a much weaker effect on the airglow intensity than on the Doppler shift (see Figure 4 and Table). Therefore, the entire collected dataset can be used for photometric calibration of the interferometer.

The calibration involves comparing modeled and FPI-measured integral airglow intensities. To do this, we display the received dataset in the form of a scattering diagram (Figure 5) with data from the zenith and northerly directions. Assuming the linear nature of the dependence of the modeled intensities Y on those measured by FPI X, we can introduce linear regression coefficients as $Y=aX+b$ and find their values with the least squares method. For this purpose, we used the Scipy Linregress library [Zwillinger, Kokoska, 2000]. The coefficient $b=-0.019\pm1.515$ is small as compared to FPI readings, so it can be equated to zero. The coefficient $a=0.529\pm0.018$ R/rel.unit expressing the slope of the trend line is the desired calibration coefficient.

DISCUSSION

The night increases in N_e discussed in this paper (see Figure 1) are unsatisfactorily reconstructed by numerical modeling, specifically, by PIM ISTP. Ionospheric neutral component parameters required for PIM are determined by semi-empirical MSIS and HWM models, which probably ignore some serious regional features. Moreover, the current version of PIM accounts only for the horizontal wind effect, calculated in HWM, ignoring the vertical component of neutral particle motion. Thus, the neutral wind model requires expanding and taking into account the regional features of the motion of the neutral atmosphere, as well as its vertical motion.

The vertical N_e profile variations observed in IISR data can be explained by a change of the direction of the neutral wind. The case under study shows that in addition to the horizontal wind it is necessary to consider the vertical air motion in the upper atmosphere. The observed descent of ionospheric plasma can be provided by the meridional wind directed into the polar region and moving charged particles along the magnetic field line downward. Thus, the

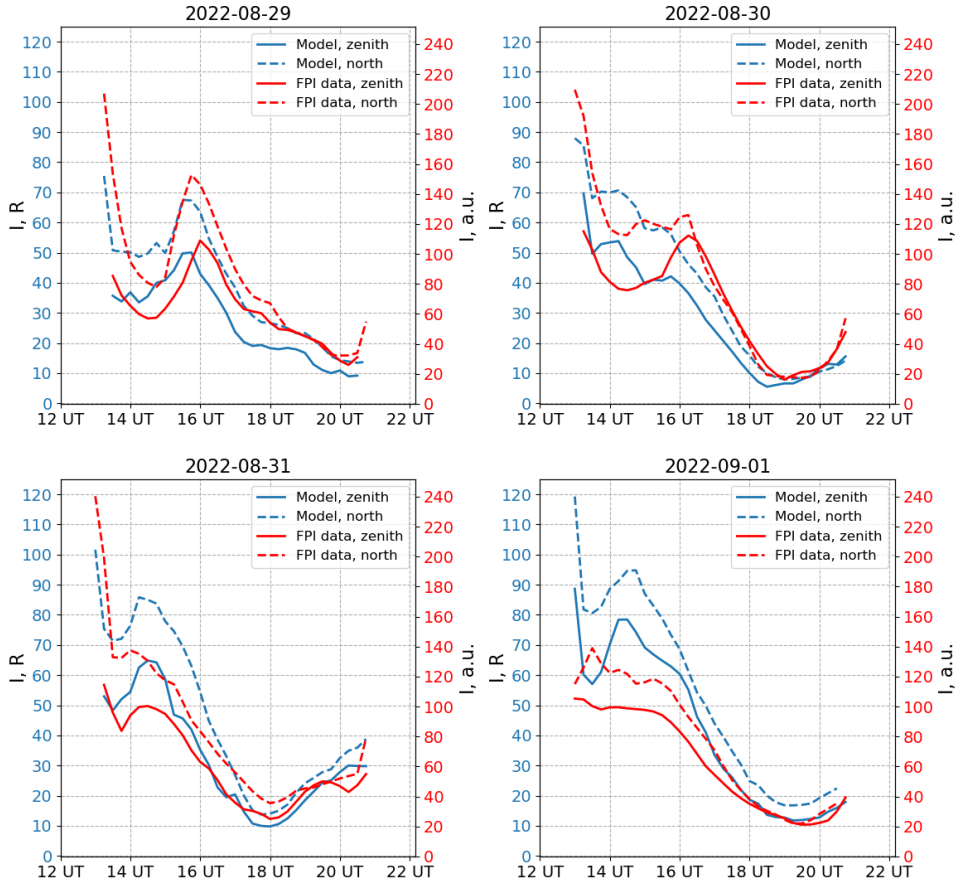

Figure 4. Comparison of the integral intensity obtained by modeling based on IISR data (blue curves) and the intensity measured by FPI (red curves). Solid curves correspond to the zenith direction; dashed ones, to the northerly direction

Correlation coefficients of night 630 nm line intensity variations modeled and measured by FPI

Date	Pearson coefficient *r*	Spearman coefficient ρ
Aug. 29, 2022	0.869	0.897
Aug. 30, 2022	0.901	0.869
Aug. 31, 2022	0.942	0.962
Sept. 01, 2022	0.969	0.938

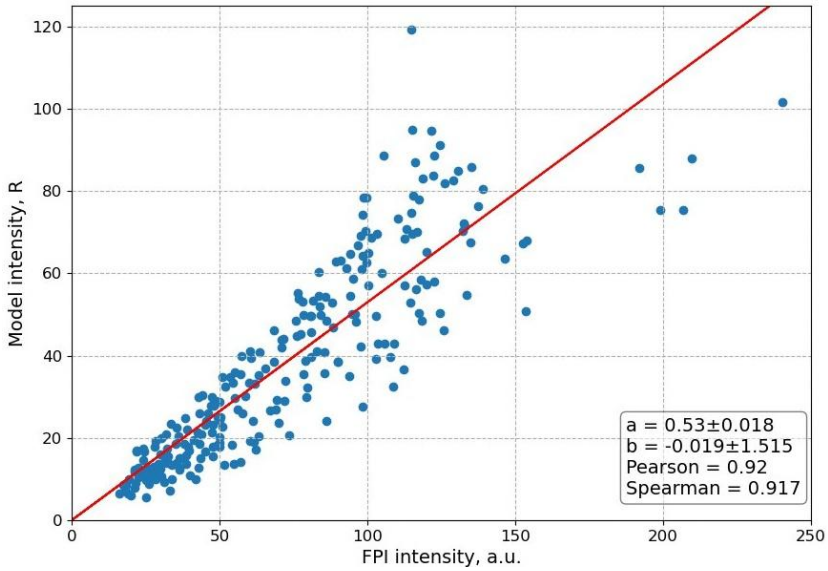

Figure 5. Ratio of the model 630 nm integral intensity obtained from IISR data to that measured by FPI (zenith and northerly directions) for August 28 – September 1, 2022.

polar meridional wind at night can increase the concentration of charged particles at low altitudes. The calculated meridional wind (see Figure 2, *b*, orange dashed curve) is southward at night (negative values) and does not allow observing the effects of downward plasma drift along the field line. On the contrary, the calculated concentrations demonstrate an increase in the maximum at dawn and this is consistent with the wind direction. Despite the fact that the meridional wind measured by FPI is also southward throughout the night (see Figure 2, *b*, orange solid curve), consideration of vertical motion of atmospheric layers provides insight into the observed decrease in the height of the ionospheric maximum in the first half of the night. This result through direct observations confirms the previous conclusion that vertical air motion should be taken into account to describe the dynamics of the maximum plasma concentration, drawn by analyzing average seasonal diurnal wind variations, obtained by FPI, and the ionospheric F-layer parameters from the ionosonde [Vasilyev et al., 2020].

When discussing the nature of the observed phenomenon, it is necessary to return to the phenomenon of the midnight temperature maximum (MTM) mentioned in Introduction. Historically, MTM was detected in the near-equatorial ionosphere (±15°) and was attributed to a change of the direction of the meridional wind; it was also observed to spread to midlatitudes [Colerico, Mendillo, 2002]. Mesquita et al. [2018] recorded MTM manifestations up to 45° N without limitations on latitude, which means that their recording remains possible for the latitudes of ISTP SB RAS optical and radiophysical observatories. The night increases in the airglow concentration and intensity analyzed in this work are in good agreement with the previously described MTM manifestations. Thus, we can assume that in this case MTM has first been identified in observations at 52° N. It is worth noting that the main control parameter in both cases is the neutral wind; the role of vertical motion of neutrals should be carefully considered when studying this phenomenon.

The dominant role of dissociative recombination in oxygen excitation at night, shown by numerical modeling, allowed us to estimate the airglow intensity from ionospheric parameters determined by IISR. The calibration coefficient calculated in this work needs to be further refined using a larger dataset of measurements and be supported by data from other radiophysical instruments. However, even in its current form, the proposed simple method can be used to estimate intensities and to convert FPI data from relative units to rayleigh, avoiding the complex procedure for fully accounting for all possible plasma-chemical processes [Duann et al., 2024]. The coefficient value is 0.529 R/rel.unit; the variance ±0.018 R/rel.unit is ~3 % of the coefficient, which is within the FPI measurement accuracy. In the future, this will make it possible to combine the phenomena observed by various optical instruments into a single database, which will significantly advance the ISTP SB RAS instrumental potential.

CONCLUSION

Consistent observations of the same atmospheric region by diverse optical and radiophysical methods provide wide possibilities both for expanding the field of collecting information on observed phenomena and for calibrating individual instruments. The phenomenon of night increase in N_e observed by IISR described in our work agrees well with the 630 nm airglow variations recorded by NHC RAS FPI. The presented data points to the decisive role of the neutral wind in developing the observed phenomenon and indirectly indicates the mechanism responsible for the formation of the midnight maximum temperature detected by other researchers in different regions of Earth. We have shown that it is necessary to develop descriptive methods of neutral atmosphere dynamics, in particular, to refine the currently widely used horizontal wind model HWM. In addition, such studies must take into account the vertical motion of the upper atmosphere, which is often ignored.

The results of the work are important for the development of the ISTP SB RAS instrumentation and for the study of the features of ionospheric dynamics in the Siberian region. We have demonstrated that it is essential to correctly calculate and consider the neutral wind in the problems of modeling, forecasting, and analyzing N_e variations. In the future, we suppose that new data will be accumulated and analyzed, which contains the same features of simultaneous increases in the 630 nm atomic oxygen emission intensity and in N_e in the same atmospheric region. It is interesting to analyze data for different levels of solar activity, to employ additional facilities for observation of atmospheric parameters, satellite data, as well as other models.

The work was financially supported by the Ministry of Science and Higher Education of the Russian Federation (Subsidy No. 075-GZ/Ts3569/278).

The results were obtained using the Unique Research Facilities “Optical Instruments” [https://ckp-rf.ru/catalog/usu/4138180/] and “Irkutsk Incoherent Scatter Radar” [https://ckp-rf.ru/catalog/usu/77733/].

REFERENCES

Alken P., Maus S., Emmert J., Drob D.P. Improved horizontal wind model HWM07 enables estimation of equatorial ionospheric electric fields from satellite magnetic measurements. *Geophys. Res. Lett*. 2008, vol. 35, no. 11. DOI: 10.1029/2008GL033580.

Alsatkin S.S., Medvedev A.V., Ratovsky K.G. Some peculiarities in the ionosphere dynamics near the ionization maximum from Irkutsk incoherent scatter radar data for low and moderate solar activities. *Sol.-Terr. Phys.* 2015, vol. 1, no. 3, pp. 28–36, DOI: 10.12737/11450.

Afraimovich E.L., Zherebtsov G.A., Perevalova N.P. *Seismo-Ionospheric and Seismo-Electromagnetic Processes in Baikal Rift Valley.* Novosibirsk, SB RAS, 2012, 304 p. (In Russian).

Berrington K.A., Burke P.G. Effective collision strengths for forbidden transitions in e − N and e − O scattering, *Planet. Space Sci*. 1981, vol. 29, iss. 3, pp. 377–381. DOI: 10.1016/0032-0633(81)90026-X.

Bilitza D., Pezzopane M., Truhlik V., et al. The International Reference Ionosphere model: A review and description of an ionospheric benchmark. *Rev. Geophys*. 2022, vol. 60, iss. 4. DOI: 10.1029/2022RG000792.

Bryunelli B.E., Namgaladze A.A. *Ionosphere Physics*. Moscow, Nauka, 1988, 526 p. (In Russian).

Cedric M.V., Podlesny A.V., Kurkin V.I. Three-position reception of signals with linear frequency modulation during slightly-inclined ionospheric sounding. *Proc. of All-Russian Open Scientific Conference "Modern Problems of Waves Remote Sensing, Radiolocation, Propagation and Diffraction"],* Murom, 2022, pp. 223–229. DOI: 10.24412/2304-0297-2022-1-223-229. (In Russian).

Colerico M.J., Mendillo M. The current state of investigations regarding the thermospheric midnight temperature maximum (MTM). *J. Atmos. Sol.-Terr. Phys*. 2002, vol. 64, pp. 1361–1369.

Doering J.P. Absolute differential and integral electron excitation cross sections for atomic oxygen: 9. Improved cross section for the $^3P \rightarrow {}^1D$ transition from 4.0 to 30 eV. *J. Geophys. Res.* 1992, vol. 97, iss. A12, pp. 19531–19534. DOI: 10.1029/92JA02007.

Duann Y., Chang L.C., Chiu Y.-C., et al. Atomic oxygen ion retrieval from 630.0 nm airglow during geomagnetically quiet periods: a mid-latitude case study near Irkutsk. *Geoscience. Lett.* 2024, vol. 11, no. 55. DOI: 10.1186/s40562-024-00370-6.

Emmert J.T., Jones Jr. M., Siskind D.E., et al. NRLMSIS 2.1: An empirical model of nitric oxide incorporated into MSIS. *J. Geophys. Res.: Space Phys*. 2022, vol. 127, iss. 10. DOI: 10.1029/2022JA030896.

Garcia F.J., Kelley M.C., Makela J.J., Huang C.-S. Airglow observations of mesoscale low-velocity traveling ionospheric disturbances at midlatitudes. *J. Geophys. Res.* 2000, vol. 105, iss. A8, pp. 18407–18415. DOI: 10.1029/1999JA000305.

Grigoryev S.A., Latyshev K.S. Non-stationary processes in geomagnetic force tubes. Numerical methods analysis. *Matematicheskoe modelirovanie* [Mathematical modeling]. 1989, vol. 1, iss. 9, pp. 141–150. (In Russian).

Harding B.J., Gehrels T.W., Makela J.J. Nonlinear regression method for estimating neutral wind and temperature from Fabry-Perot interferometer data. *App. Optics.* 2014, vol. 53, iss. 4, pp. 666–673. DOI: 10.1364/AO.53.000666.

Hargreaves J. K. *Upper Atmosphere and Solar-Terrestrial Interactions: Introduction to Near-Earth Space Physics.* Leningrad, Gidrometeoizdat, 1982, 352 p. (In Russian).

Kernahan J.H., Pang P.H.-L. Experimental determination of absolute A coefficients for "forbidden" atomic oxygen lines. *Can. J. Phys*. 1975, vol. 53, iss. 5, pp. 455–458.

Korenkov Yu.N., Klimenko V.V., Förster M., et al. Global modelling study (GSM TIP) of the ionospheric effects of excited N2, convection and heat fluxes by comparison with EISCAT and satellite data for 31 July 1990. *Ann. Geophys.* 1996, vol. 14, iss. 12, pp. 1362–1374. DOI: 10.1007/s00585-996-1362-2.

Krinberg I.A., Tashcilin M.A. *Ionosfera i plasmosfera* [Ionosphere and Plasmasphere]. Moscow: Nauka, 1984, 189 p. (In Russian).

Link R., Cogger L. A reexamination of the OI 6300 angstrom nightglow. *J. Geophys. Res*. 1988, vol. 93, iss. A9, pp. 9883–9892.

Mantas G.P. Large 6300 Å airglow intensity enhancements observed in ionosphere heating experiments are excited by thermal electrons. *J. Geophys. Res.* 1994, vol. 99, iss. A5, pp. 8993–9002. DOI: 10.1029/94JA00347.

Mesquita R.L.A., Meriwether J.W., Makela J.J., et al. New results on the mid-latitude midnight temperature maximum. *Ann. Geophys.* 2018, vol. 36, iss. 2, pp. 541–553. DOI: 10.5194/angeo-36-541-2018.

Mikhalev A.V. Seasonal and interannual variations in the [OI] 630 nm atmospheric emission as derived from observations over Eastern Siberia in 2011–2017. *Sol.-Terr. Phys.* 2018, vol. 4, iss. 2, pp. 58–62. DOI: 10.12737/stp-42201809.

Namgaladze A.A., Zaharov L.P., Namgaladze A.N. Ionosphere storms numerical modeling. *Geomagnetizm i aeronomia* [Geomagnetism and aeronomy]. 1981, vol. 21, iss. 2, pp. 259–265. (In Russian).

Otsuka Y., Kadota T., Shiokawa K., et al. Optical and radio measurements of a 630 nm airglow enhancement over Japan on 9 September 1999. *J. Geophys. Res*. 2003, vol. 108, iss. A6, p. 1252. DOI: 10.1029/2002JA009594.

Picone J.M., Hedin A.E., Drob D.P., Aikin A.C. NRLMSISE-00 empirical model of the atmosphere: Statistical comparisons and scientific issues. *J. Geophys. Res*. 2002, vol. 107, iss. A12, p. 1468. DOI: 10.1029/2002JA009430.

Podlesny S.V., Devyatova E.V., Saunkin A.V., Vasilyev R.V. Comparing methods to estimate cloud cover over the Baikal natural territory in December 2020. *Sol.-Terr. Phys.* 2022, vol. 8, iss. 4, pp. 95–102. DOI: 10.12737/stp-84202210.

Ratovsky K.G., Oinats A.V. Local empirical model of ionospheric plasma density derived from digisonde measurements at Irkutsk. *Earth, Planets and Space*. 2011, vol. 63, pp. 351–357. DOI: 10.5047/eps.2011.03.002.

Rishbeth H. Basic physics of the ionosphere: a tutorial review. *J. of the Institution of Electronic and Radio Engineers*. 1988, vol. 58, iss. 6S, pp. 207–223. DOI: 10.1049/jiere.1988.0060.

Shcherbakov A.A., Medvedev A.V., Kushnarev D.S., et al. Calculation of meridional neutral winds in middle latitudes from the Irkutsk Incoherent Scatter Radar data. *Sol.-Terr. Phys.* 2015, vol. 1, no. 3, pp. 37–48. DOI: 10.12737/10962.

Shefov N.N., Semenov A.I., Khomich V.Yu. *Upper atmosphere airglow — its structure and dynamics indicator*. Moscow: GEOS, 2006, 741 p. (In Russian).

Shepherd G.G., Siddiqi N.J., Wiens R.H., Zhang S. Airglow measurements of possible changes in the ionosphere and middle atmosphere. *Adv. Space Res*. 1997, vol. 20, iss. 11, pp. 2127–2135. DOI: 10.1016/S0273-1177(97)00605-4.

Tashchilin A.V., Leonovich L.A. Modeling nightglow in atomic oxygen red and green lines under moderate disturbed geomagnetic conditions at midlatitudes. *Sol.-Terr. Phys.* 2016, vol. 2, iss. 4, pp. 94–106. DOI: 10.12737/24276.

Van Zandt T.E. III-3 — The neutral atmosphere and the quiet ionosphere. *International Geophysics*. 1967, vol. 11, iss. 1, pp. 509–559. DOI: 10.1016/B978-0-12-480301-5.50015-X.

Vasilyev R.V., Artamonov M.F., Beletsky A.B., et al. Registering upper atmosphere parameters in East Siberia with Fabry — Perot interferometer KEO Scientific "Arinae". *Sol.-Terr. Phys.* 2017, vol. 3, iss. 3, pp. 61–75. DOI: 10.12737/stp-33201707.

Vasilyev R.V., Artamonov M.F., Beletsky A.B., et al. Scientific goals of optical instruments of the National Heliogeophysical Complex. *Sol.-Terr. Phys.* 2020, vol. 6, iss. 2, pp. 84–97, DOI: 10.12737/stp-62202008.

Watanabe K., Ashour-Abdalla M., Sato T. A numerical model of magnetosphere-ionosphere coupling: Preliminary results. *J. Geophys. Res*. 1986, vol. 91, iss. A6, pp. 6973–6978. DOI: 10.1029/JA091iA06p06973.

Weinstock J. Theory of enhanced airglow during ionospheric modifications. *J. Geophys. Res*. 1975, vol. 80, iss. 31, pp. 4331–4345. DOI: 10.1029/JA080i031p04331.

Zherebtsov G.A. Complex of heliogeophysical instruments of new generation. *Sol.-Terr. Phys.* 2020, vol. 6, iss. 2, pp. 3–13. DOI: 10.12737/stp-62202001.

Zherebtsov G.A., Zavorin A.V., Medvedev A.V., et al. Irkutsk incoherent scatter radar. *Radiotehnika i elektronika* [Radio

Engineering and Electronics]. 2002, vol. 47, no. 11, pp. 1339–1345. (In Russian).

Zwillinger D., Kokoska S. *CRC Standard Probability and Statistics. Tables and Formulae*. New York, Chapman & Hall, 2000, 537 p.

URL: https://ckp-rf.ru/catalog/usu/4138180/ (accessed October 2, 2025).

URL: https://ckp-rf.ru/catalog/usu/77733/ (accessed October 2, 2025).

Original Russian version: Vasiliev R.V., Edemskiy I.K., Shelkov A.D., Artamonov M.F., Alsatkin S.S., Evseev U.N., Lebedev V.P., Tashlykov V.P., Tashchilin A.V., Timchenko A.V. published in Solnechno-zemnaya fizika. 2025, vol. 11, no. 3, pp. 33–43. DOI: 10.12737/szf-114202502.

How to cite this article

Vasiliev R.V., Edemskiy I.K., Shelkov A.D., Artamonov M.F., Alsatkin S.S., Evseev U.N., Lebedev V.P., Tashlykov V.P., Tashchilin A.V., Timchenko A.V. Analyzing the behavior of mid-latitude upper atmosphere ionospheric plasma and airglow I630 from IS radar and Fabry—Perot interferometer data. *Sol.-Terr. Phys.* 2025, vol. 11, iss. 4, pp. 29–38. DOI: 10.12737/stp-114202502.